Supplementary Table 1. Baseline demographic and laboratory data of the study population. Related to Figure 1.

	Non-alcoholic controls (n=33)	Patients with alcohol use disorder and liver disease (n=36)
Gender (male), n (%)	15 (45.5)	19 (52.8)
Age (years), n=69	34.0 (16.0)	50.0 (16.3)
BMI (kg/m^2), n=60	22.0 (2.5)	24.9 (6.9)
AST (IU/L), n=36		49.5 (56.5)
ALT (IU/L), n=36		37.0 (31.3)
GGT (IU/L), n=36		68.5 (146.3)
AP (IU/L), n=36		78.0 (44.3)
Bilirubin (mg/dL), n=36		0.4 (0.4)
Albumin (g/dL), n=36		4.5 (0.3)
INR, n=35		1.0 (0.1)
Creatinine (mg/dL), n=36		0.70 (0.20)
CAP (dB/m), n=36		276.5 (83.3)
Stiffness (kPa), n=36		5.95 (2.33)
Fibrosis stages F2-F4, n (%)		7 (19.4)

Values are presented as median and interquartile range in parentheses. The number of subjects for which data were available is indicated in the first column. ALT, alanine aminotransferase; AP, alkaline phosphatase; AST, aspartate aminotransferase; BMI, body mass index; CAP, controlled attenuation parameter; GGT, gamma-glutamyltransferase; INR, international normalized ratio.

Supplementary Table 2. Baseline demographic and laboratory data of 2 patients with liver biopsy. Related to Figure 1.

	Alcohol-associated liver disease (n=2)
Gender (male), n (%)	1 (50.0)
Age (years)	49 (4.0)
BMI (kg/m^2)	28.2 (0.5)
AST (IU/L)	90.5 (64.5)
ALT (IU/L)	125.0 (90.0)
GGT (IU/L)	305.5 (234.5)
AP (IU/L)	86.5 (7.5)
Bilirubin (mg/dL)	0.8 (0.3)
Albumin (g/dL)	4.8 (0.1)
INR	1.0 (0.0)
Creatinine (mg/dL)	0.78 (0.04)
CAP (dB/m)	331.5 (21.5)
Stiffness (kPa)	8.75 (0.55)
Fibrosis stages F2-F4, n (%)	2 (100.0)

Values are presented as median and interquartile range in parentheses. ALT, alanine aminotransferase; AP, alkaline phosphatase; AST, aspartate aminotransferase; BMI, body mass index; CAP, controlled attenuation parameter; GGT, gamma-glutamyltransferase; INR, international normalized ratio.

Supplementary Table 3. Quantitative PCR primers used in this study. Related to Figure 3, 4, 5, 6, 7.

Gene	Application	Sequence
Mouse *Adh1*	qRT-PCR	F: 5'-GGGTTCTCAACTGGCTATGG-3'
		R: 5'-ACAGACAGACCGACACCTCC-3'
Mouse *Cyp2e1*	qRT-PCR	F: 5'-CTTAGGGAAAACCTCCGCAC-3'
		R: 5'-GGGACATTCCTGTGTTCCAG-3'
Mouse *Il1b*	qRT-PCR	F: 5'-GGTCAAAGGTTTGGAAGCAG-3'
		R: 5'-TGTGAAATGCCACCTTTTGA-3'
Mouse F4/80	qRT-PCR	F: 5'-GGATGTACAGATGGGGGATG-3'
		R: 5'-CATAAGCTGGGCAAGTGGTA-3'
Mouse 18S	qRT-PCR	F: 5'-AGTCCCTGCCCTTTGTACACA-3'
		R: 5'-CGATCCGAGGGCCTCACTA-3'
Mouse *Cxcl1*	qRT-PCR	F: 5'-TGCACCCAAACCGAAGTC-3'
		R: 5'-GTCAGAAGCCAGCGTTCACC-3'
Mouse *Cxcl2*	qRT-PCR	F: 5'-AAAGTTTGCCTTGACCCTGAA-3'
		R: 5'-CTCAGACAGCGAGGCACATC-3'
Mouse *Ccl2*	qRT-PCR	F: 5'-ATTGGGATCATCTTGCTGGT-3'
		R: 5'-CCTGCTGTTCACAGTTGCC-3'
Mouse *Tnfa*	qRT-PCR	F: 5'-AGGGTCTGGGCCATAGAACT-3'
		R: 5'-CCACCACGCTCTTCTGTCTAC-3'
Fungal 18S rRNA	qRT-PCR	F: 5'-GGRAAACTCACCAGGTCCAG-3'
		R: 5'-GSWCTATCCCCAKCACGA-3'

Candida spp.[1]	qRT-PCR	F: 5’-CAACGGATCTCTTGGTTCTC-3’ R: 5'-CGGGTAGTCCTACCTGATTT-3'

18

Supplementary Figure Legends

Figure S1. *C. albicans*-reactive Th17 cells migrate to and are present in the liver of patients with alcohol use disorder and liver disease. Related to Fig. 1.

(A) Gating strategies of fungus-reactive $CD154^+CD45RA$-memory $CD4^+$ T cells and cytokine production upon enrichment by ARTE. (B) Scatterplot demonstrating Pearson correlation between the percentage of *C. albicans*-reactive Th17 cells and liver stiffness (in kPa) in patients with alcohol use disorder and liver disease (n=36). (C) Study design for single-cell RNA and TCR sequencing of *C. albicans*-stimulated T cells from PBMCs, as well as bulk TCR sequencing from liver biopsies and peripheral $CD4^+$ T cells. *C. albicans*-stimulated T cells were magnetically isolated based on dual expression of CD154 and CD69 (ARTE) from patients with alcohol-associated liver disease after stimulation with whole *C. albicans* lysates, further purified by FACS sorting, and subjected to single-cell RNA and TCR sequencing. Single-cell RNA sequencing combined with TCR sequencing provides the transcriptomic description and clonal composition of *C. albicans*-stimulated T cells. For bulk TCR sequencing, RNA is extracted from liver biopsies and total $CD4^+$ T cells from blood of the same individuals as the single-cell RNA and TCR sequencing. Bulk TCR sequences of liver biopsies and peripheral $CD4^+$ T cells were compared with the *C. albicans*-stimulated single-cell TCR sequences to identify shared clonotypes. Created with Biorender.com.

Figure S2. *C. albicans*-activated Th17 cells in mice on a control diet and migration from mesenteric lymph nodes to liver. Related to Fig. 2

(A-D) C57BL/6 mice were fed chronic plus binge ethanol diet (ethanol) or isocaloric diet (control). Fungus-activated Th17 cells in mesenteric lymph nodes, portal vein blood, and liver were detected after isolation of mononuclear cells, following 6 hrs *ex vivo* stimulation with *C. albicans* or *S. cerevisiae* lysate. (A) Flow cytometry plots of $IL17A^+CD154^+$ cells among $CD4^+$ T cells from mice fed a control diet. Gating strategies of fungus-activated Th17 cells in mesenteric lymph nodes (B), portal vein blood (C), and liver (D). (E-F) Kaede mice were fed a chronic plus binge ethanol diet (ethanol) or isocaloric diet (control). Fungus-activated Th17 cells in liver were detected after isolation of mononuclear cells, following 6 hrs *ex vivo* stimulation with *C. albicans* or *S. cerevisiae* lysate. (E) Flow

cytometry plots of photoconverted and migrated (Kaede red) cells from hepatic mononuclear cells. (F) Gating strategies for fungus-activated Th17 cells in photoconverted (Kaede red) cells.

Figure S3. Nystatin does not induce hepatic inflammatory cytokines and does not significantly affect the composition of the bacterial microbiota. Related to Fig. 3.
C57BL/6 mice were placed on a chronic Lieber DeCarli diet or control diet for 8 weeks. Diets were supplemented with or without nystatin for the last 10 days. (A) Hepatic levels of *Il1b*, *Cxcl1*, *Cxcl2*, *Tnfa* and *Ccl2* mRNA in mice fed a control diet. Figure S3A was conducted in 2 independent experiments. Results are expressed as mean±SEM. Fold change was calculated relative to vehicle-treated mice on control diet. (B-C) 16S rRNA sequencing of cecum samples was performed. Principal Coordinates Analysis (PCoA) was used to show beta diversity between the groups based on the abundance of 66 bacterial at the genus level. (D) Relative abundances of top 10 genera are shown.

Figure S4. *Candida*-specific TCR transgenic mice develop more severe ethanol-induced liver disease. Related to Fig. 4 and 5.
(A) Gating strategies for *Candida*-specific Th17 cells in *Rag1*$^{-/-}$/*CaTCRtg* mice. (B) Gating strategies for *Rag1*$^{-/-}$ mice. (C) Timeline of adoptive transfer experiments of *ex vivo C. albicans*-primed T cells from *Candida*-specific TCR transgenic mice (*Rag1*$^{-/-}$*/CaTCRtg*) or non-transgenic control mice into wild-type mice. (D) Gating strategies for Thy1.1^{+} CD4^{+} Vα2^{+} hector T cells in livers of recipient mice that received *C. albicans*-primed T cells from *Rag1*$^{-/-}$*/CaTCRtg* mice (upper panel) or wild-type C57BL/6 mice (lower panel).

Figure S5. *Candida*-specific TCR transgenic hector T cells promote ethanol-induced liver disease. Related to Fig. 5.
(A) Diagram of adoptive transfer of non-primed *Rag1*$^{-/-}$*/CaTCRtg* hector T cells to mice. CD4^{+} T cells from *Candida*-specific TCR transgenic mice (*Rag1*$^{-/-}$/*CaTCRtg*) and C57BL/6 donor mice were injected intravenously to C57BL/6 mice (day 13 of chronic plus binge ethanol feeding). Created with BioRender.com. (B) Serum levels of ALT. (C) Hepatic triglyceride content. (D) Representative oil red O-stained liver sections (scale bar, 100

μm). (E) Hepatic levels of *Il1b* mRNA. (F) Serum levels of ethanol. (G-H) Hepatic levels of *Cyp2e1* and *Adh1* mRNAs. Figure S4 E-L was conducted in 2 independent experiments. Results are expressed as mean±SEM. Fold change was calculated relative to mice that adoptively transferred with $CD4^+$ T cells from C57BL/6 mice. *P* values determined by 2-sided Student t test. *P<0.05.

Figure S6. *C. albicans*-primed polyclonal T cells promote ethanol-induced liver disease in mice. Related to Fig. 6.

(A) Timeline of adoptive transfer experiments of *ex vivo* fungi-primed polyclonal $CD4^+$ T cells to mice. (B) Gating strategies for IL17A-$eGFP^+$ cells after expansion of fungus-primed Th17 cells. (C) Gating strategies for IL17A-$eGFP^+$ cells detected in livers of recipient mice fed ethanol.

Figure S7. Bone marrow derived cells mediate the disease exacerbating effect of adoptively transferred polyclonal *C. albicans*-primed T cells. Related to Fig. 7.

(A) Diagram of adoptive transfer of *C. albicans*-primed polyclonal T cells to *IL17ra*$^{\Delta BM}$ chimeric mice. Wild-type (WT) recipient mice underwent transplantation of wild-type or *IL17ra* deficient bone marrow (*IL17ra*$^{\Delta BM}$) and fed a chronic plus binge ethanol diet. Chimeric mice were injected with *C. albicans*-primed polyclonal T cells three days before harvesting. Created with BioRender.com. (B) Serum levels of ALT. (C) Hepatic triglyceride content. (D) Representative oil red O-stained liver sections (scale bar, 100 μm). (E) Immunoblot of Il1b in liver samples. (F-G) Hepatic levels of *Cxcl1* and *Cxcl2* mRNAs. (H) Serum levels of ethanol. (I-J) Hepatic levels of *Cyp2e1* and *Adh1* mRNAs. (K-Q) *Il17ra*$^{\Delta Hep}$ and littermate *Il17ra*$^{fl/fl}$ mice were fed a chronic plus binge ethanol diet. *C. albicans*-primed polyclonal T cells were injected intravenously 3 days before harvesting. (K) Serum levels of ALT. (L) Hepatic triglyceride content. (M) Representative oil red O-stained liver sections (scale bar, 100 μm). (N) Hepatic levels of *Il1b* mRNA. (O) Serum levels of ethanol. (P-Q) Hepatic levels of *Cyp2e1*and *Adh1* mRNAs. Figure S7 A-J was conducted in 2 independent experiments. Figure S7 K-Q was conducted in 2 independent experiments. Results are expressed as mean±SEM. *P* values determined by 2-sided Student *t* test. *$P<0.05$.

Supplementary Figure 1

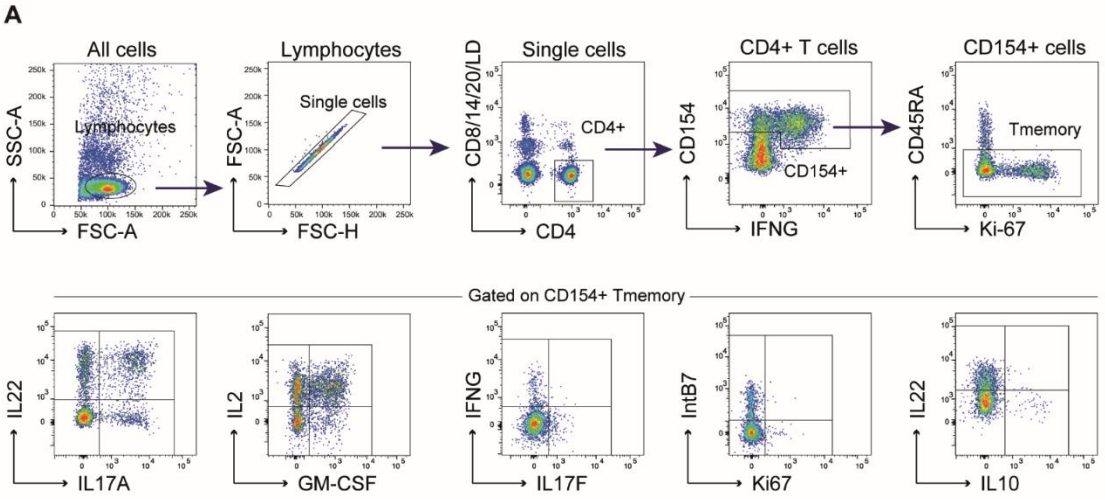

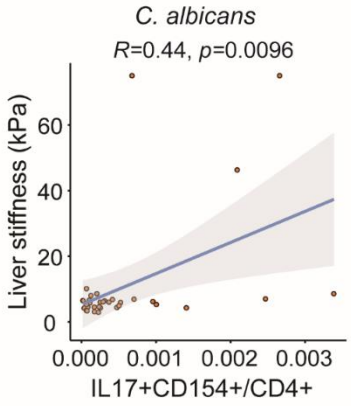

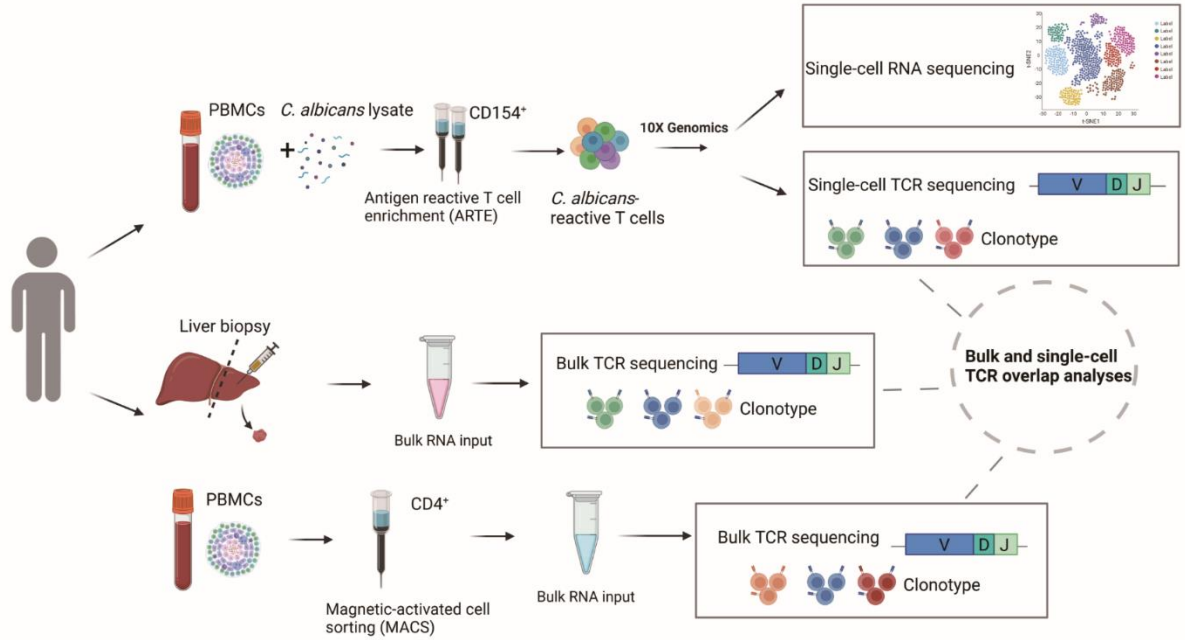

Supplementary Figure 2

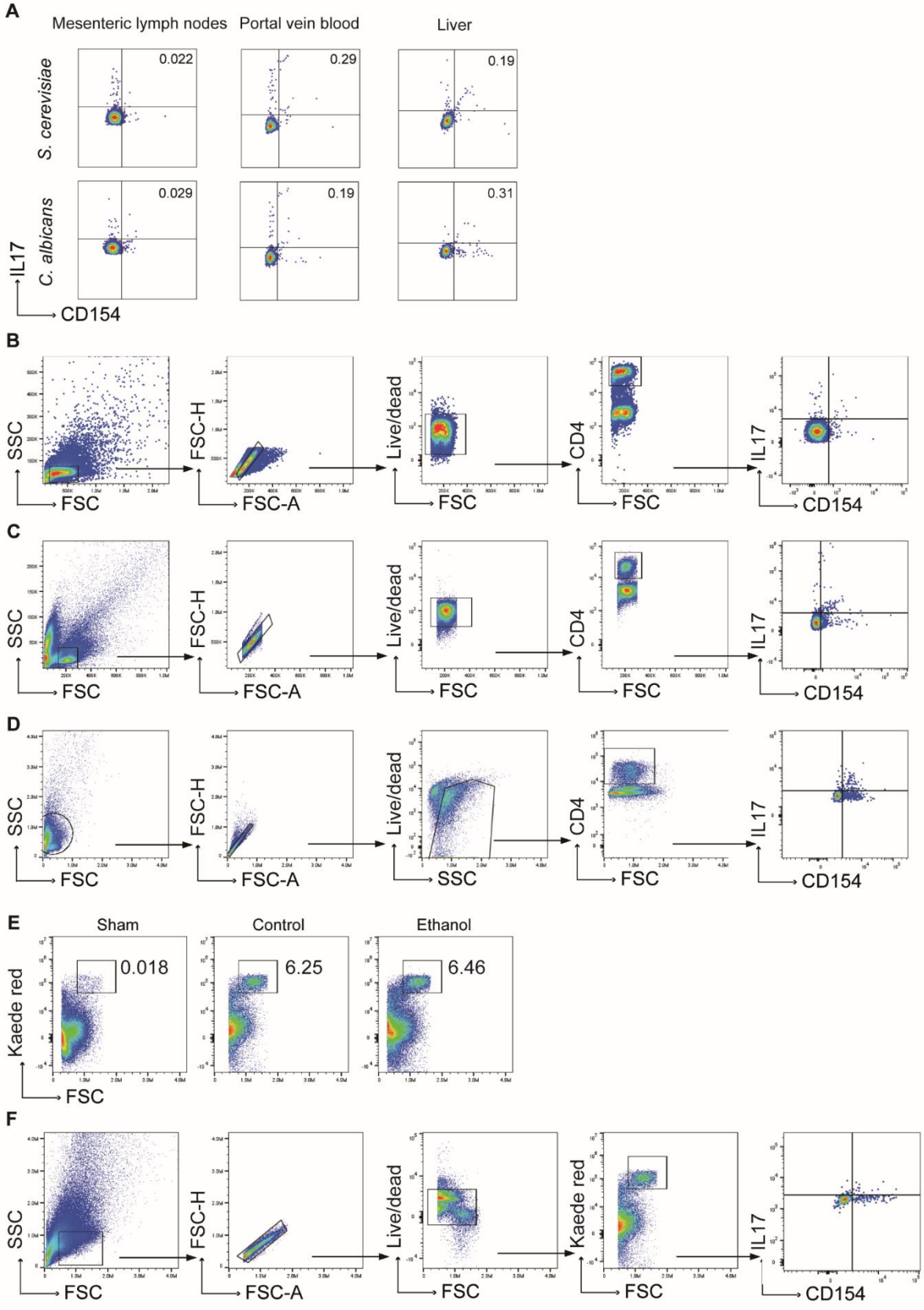

Supplementary Figure 3

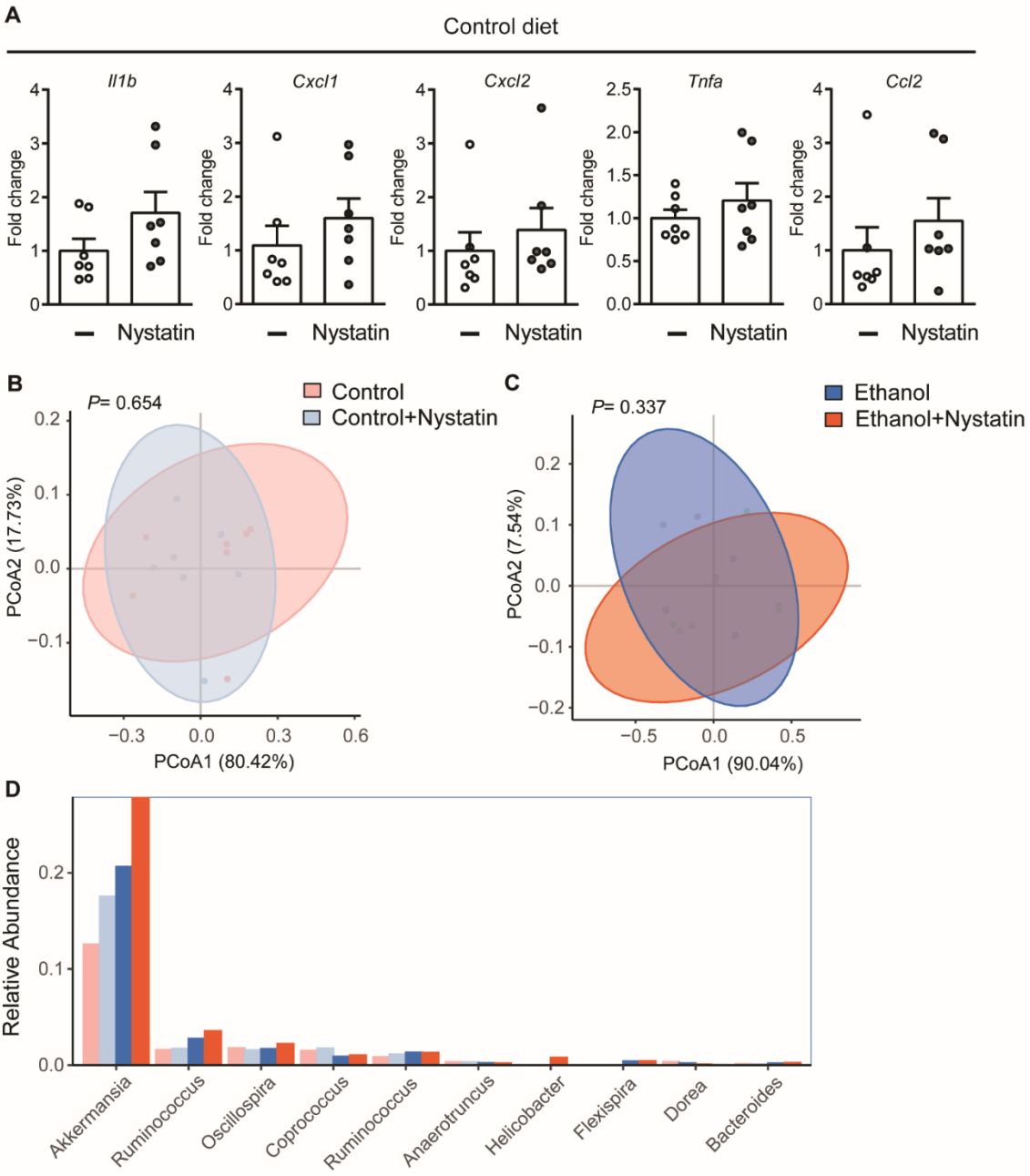

Supplementary Figure 4

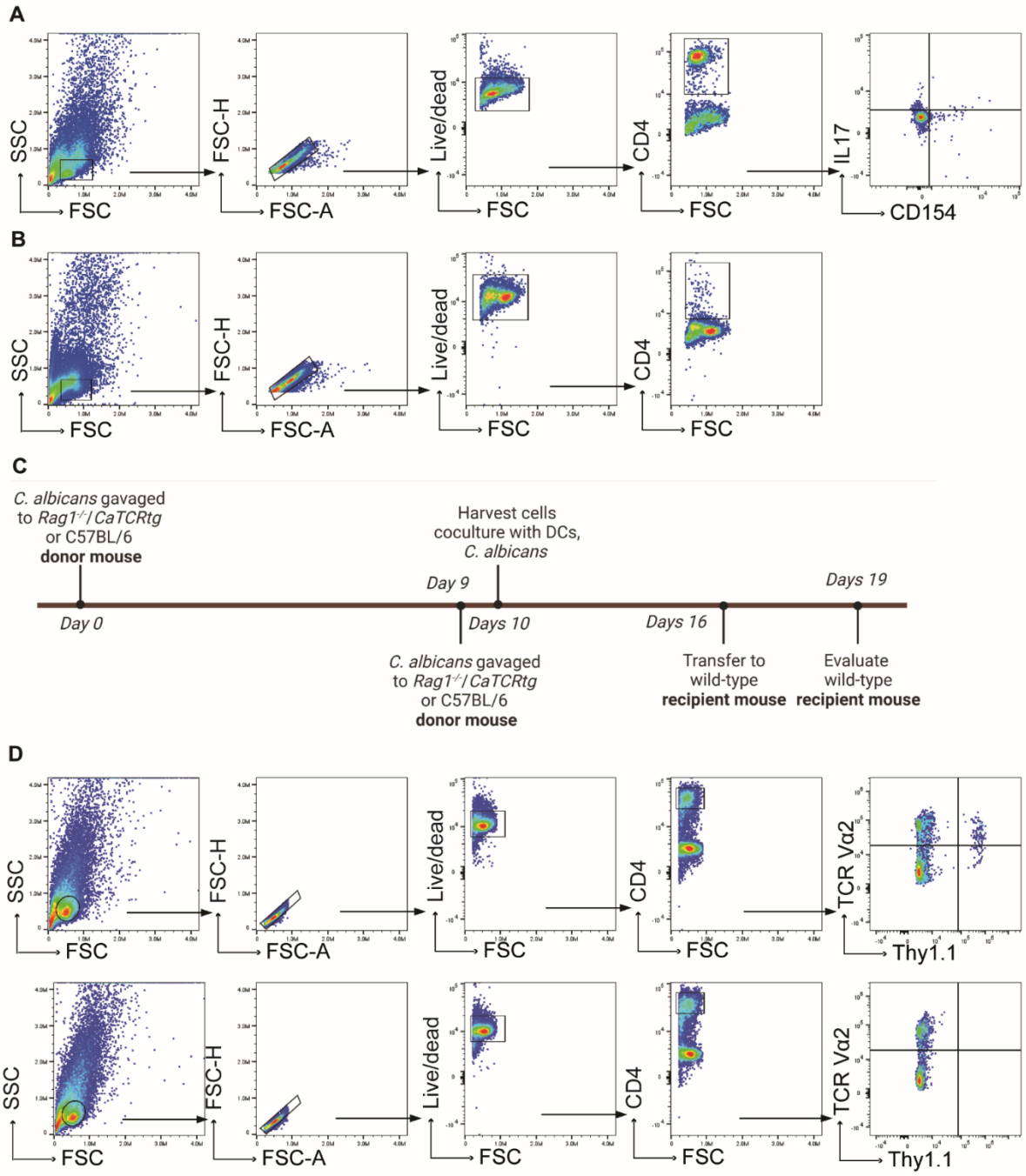

Supplementary Figure 5

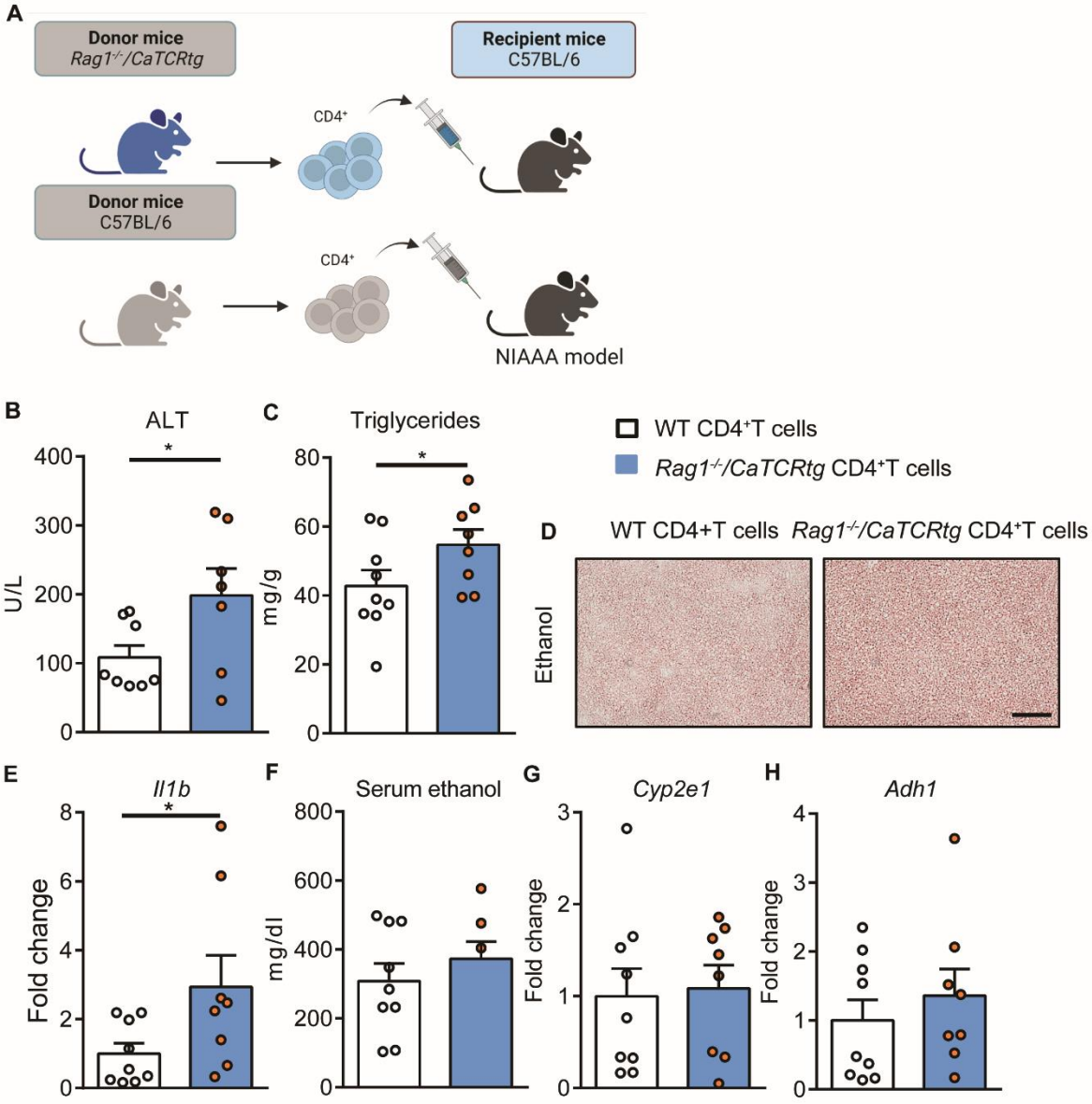

Supplemenary Figure 6

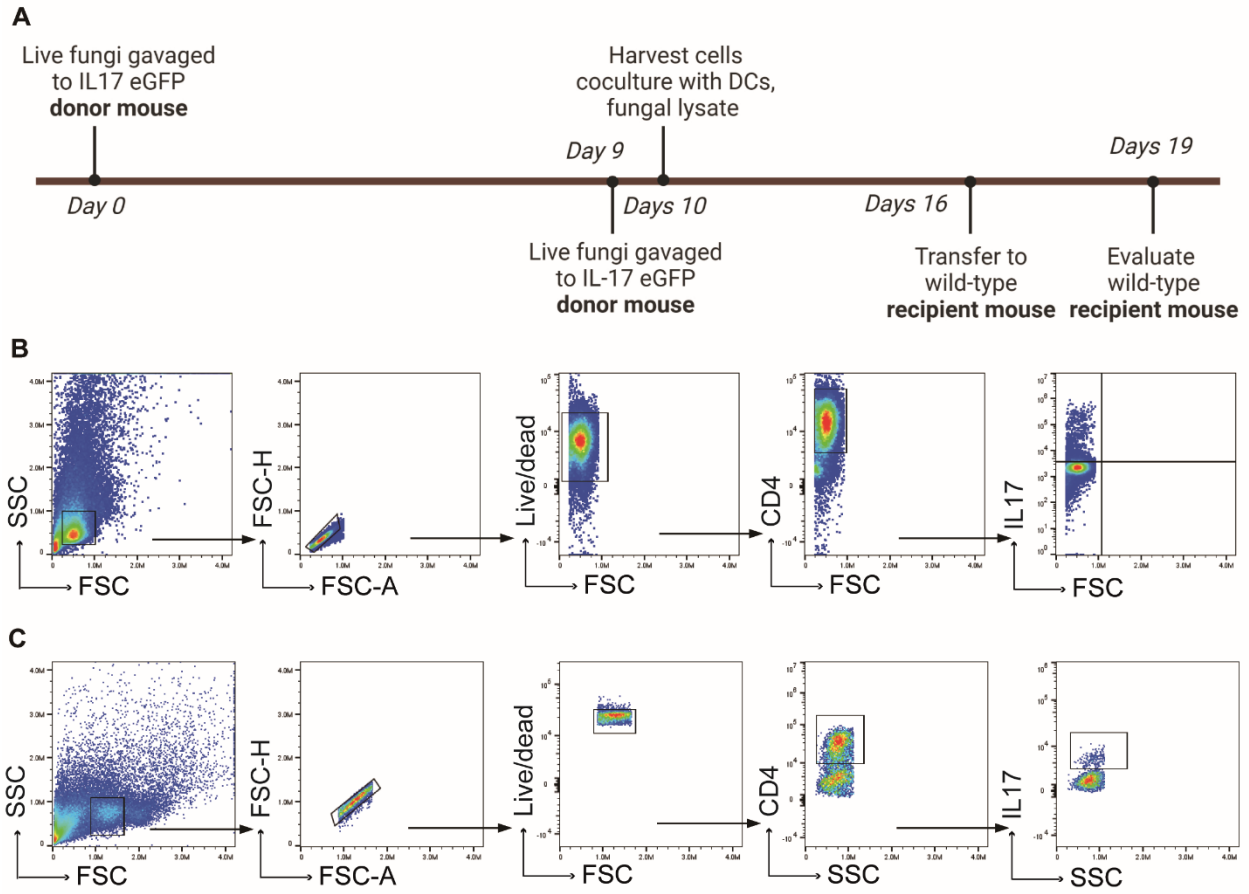

117

Supplementary Figure 7

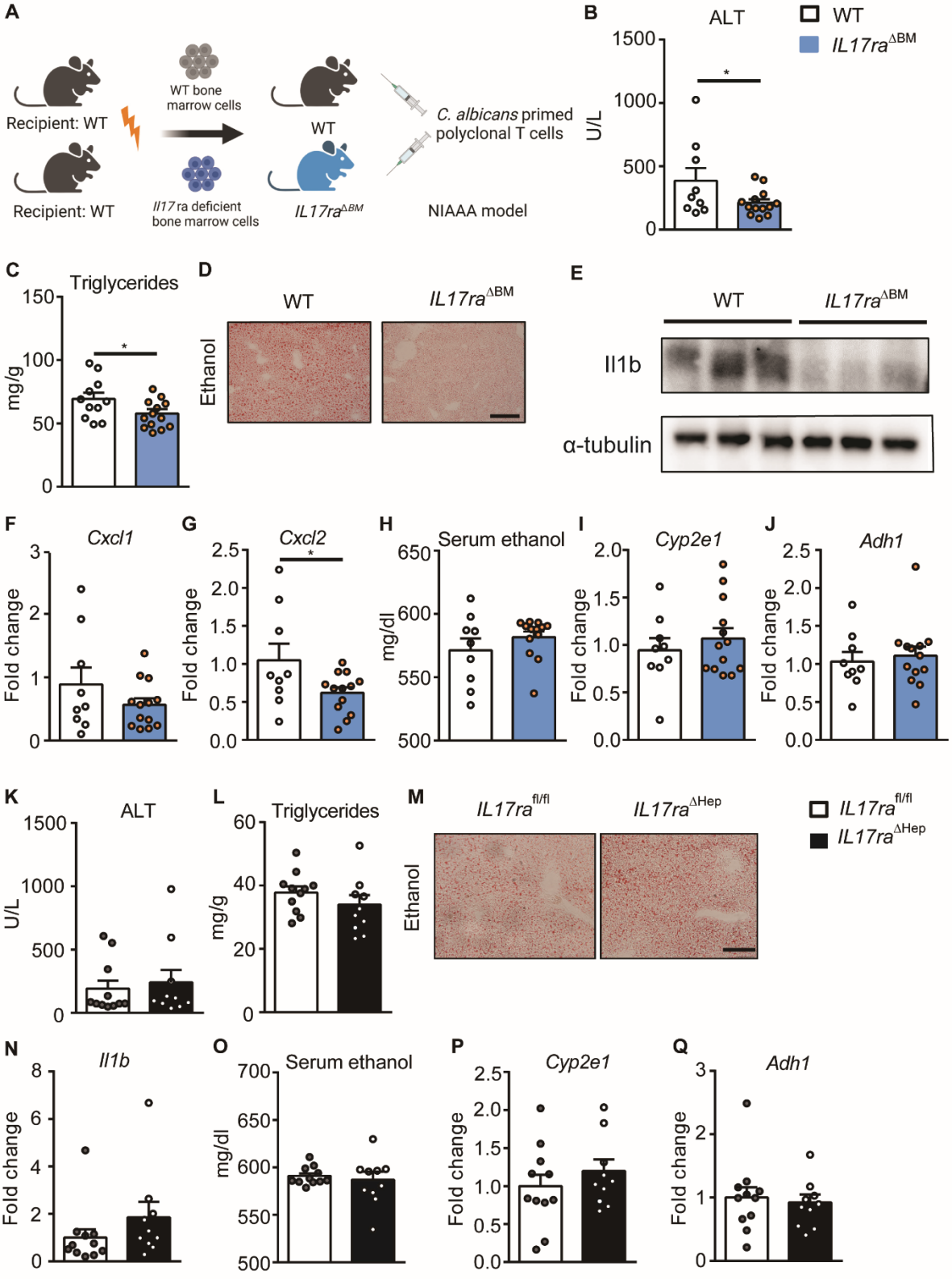

Reference

1. Zhang, J., Hung, G.C., Nagamine, K., Li, B., Tsai, S., and Lo, S.C. (2016). Development of *Candida*-Specific Real-Time PCR Assays for the Detection and Identification of Eight Medically Important *Candida* Species. Microbiol. Insights *9*, 21-28. https://doi.org/10.4137/mbi.S38517.